



ORIGINAL ARTICLE

Fabrication of virus metal hybrid nanomaterials: An ideal reference for bio semiconductor

Raja Muthuramalingam Thangavelu, Rajendran Ganapathy, Pandian Ramasamy, Kathiravan Krishnan*

Plant Molecular Virology and Nanobiotechnology Research Laboratory, Department of Biotechnology, University of Madras, Chennai, Tamil Nadu 600 025, India

Received 5 May 2018; accepted 4 July 2018
Available online 20 July 2018

KEYWORDS

Virus nanotechnology;
Virus template;
Surface biomineralization;
Virus hybrid nanomaterials;
Electrical conductivity;
Biocompatibility

Abstract Recently, Nanotechnology has made easier utilizing plant pathogens as a potential nano-material in biomedical applications. In this research work, we have exploited a devastating plant pathogenic virus of *Squash leaf curl China virus* (SLCCNV), as a nano-bio template (32 nm) to fabricate the gold and silver nanomaterials. This is achieved through the direct exposure of SLCCNV to gold chloride (HAuCl_4) and silver nitrate (AgNO_3) precursors at sunlight, resulted into SLCCNV-metallic-hybrid nanomaterials which are synthesized quick (~5 min) and eco-friendly. However, virus hybrid nanomaterials are fabricated through the nucleation and growth of metal precursors over the pH-activated capsid of SLCCNV. Under the controlled fabrication process, it produced a highly arrayed virus-metallic-hybrid nanomaterial at nanoscale size limit. Its properties are thoroughly studied through spectroscopic techniques (UV–Vis, DLS, Raman) and electron microscopy (HRTEM & FESEM). In a follow-up study of cytotoxicity assay, the virus and its fabricated nanomaterials show better biocompatibility features even at high concentrations. Finally, the electrical conductivities of virus-metallic-hybrid nanomaterials (Au & Ag) are determined by simple “lab on a chip” system and Keithley’s pico-ammeter. The result of electrical conductivity measurement revealed that hybrid nanomaterials have greater electrical conductive properties within the band-gap of semi-conductive materials. It is truly remarkable that a plant virus associated metal nanomaterials can be efficiently used as bio-semi-conductors which are the ideal one for biomedical applications.

© 2018 Production and hosting by Elsevier B.V. on behalf of King Saud University. This is an open access article under the CC BY-NC-ND license (<http://creativecommons.org/licenses/by-nc-nd/4.0/>).

Abbreviations: SLCCNV, *Squash leaf curl China virus*; VNPs, viral nanoparticles; CP, capsid; EC, electrical conductivity; AuNPs, gold nanoparticles; AgNPs, silver nanoparticles; pI, isoelectric point; SERS, surface enhanced Raman scattering; DLS, dynamic light scattering; HRTEM, high resolution transmission electron microscopy; FESEM, field emission scanning electron microscopy

* Corresponding author.

E-mail address: drkkathiravan@gmail.com (K. Krishnan).

Peer review under responsibility of King Saud University.



Production and hosting by Elsevier

1. Introduction

In recent times, biological synthesis of nanomaterials has emerged as an attractive alternative to traditional synthesis methods, which are inexpensive, free from toxic materials, cytotoxicity, carcinogenicity and potential hazards in environmental toxicity (Ai et al., 2011). So far, the presence of toxic agents on the synthesized nanomaterials has prevented its use and application in clinical fields. However, these tragic factors can be potentially controlled through biologically mediated fabrication which is currently a widespread interest in developing a clean, reliable, compatible, benign, and environment-friendly nanomaterials (Ahmad et al., 2003; Jain et al., 2011; Lewis et al., 2006; Ruoslahti, 2000; Mohanpuria et al., 2008; Philip, 2010). Biosynthesis of nanomaterials involve using an eco-friendly green chemistry based approach that employs unicellular and multicellular organisms such as actinomycetes (Ahmad et al., 2003; Sastry et al., 2003), bacteria (Joerger et al., 2001; Hussein et al., 2007; Nair and Pradeep, 2002), fungus (Dameron et al., 1989; Kuber and Souza, 2006; Mukherjee et al., 2001; Kowshik et al., 2003), plants (Kumar et al., 2011; Njagi et al., 2011; Akhtar et al., 2013), viruses (Courchesne et al., 2014; Khan et al., 2013; Lee et al., 2002; Kale et al., 2013), and yeast (Ahmed et al., 2005). Moreover, biological entities like macromolecules of peptides, lipids, and enzymes can also be utilized for the biosynthesis of nanomaterials (Klem et al., 2005; Pratibha, 2009; Kaumeel et al., 2016; Gholami shabani et al., 2015). An interesting phenomenon dealing with biological entities is their ability to act as a template in the synthesis, assembly and organization of nanometre-scale materials in the fabrication of a well-defined micro and macro scale structures (Kulkarni and Muddapur, 2014; Monaliben et al., 2015). Interestingly, studies illustrate that viruses are found to be a superior group which acts as a biotemplate for constrained material synthesis at the nanoscale to microscale (Khan et al., 2013). In recent times, viral nanoparticles (VNPs) are increasingly used as templates or scaffolds for the design of novel hybrid nanomaterials to nano-smart devices by materials science researchers (Steinmetz and Manchester, 2011). A wide variety of viral nanoparticles (VNPs) both in mammalian and plant origin have been extensively studied and implemented in biomedical technology (Young et al., 2008; Bancroft et al., 1968; Fischlechner and Donath, 2007; Lewis et al., 2006). A group of plant viruses was utilized as nanopatforms for their unique structural integrity, easy manipulation and significantly less infective to human being (Douglas and Young, 1998; Steinmetz and Manchester, 2011). In particular, because of their amazing structural diversity, capsid has been exploited as a biotemplate for material synthesis (Lee et al., 2009; Nam et al., 2006; Mao et al., 2004; Merzlyak et al., 2006). The capsid or protein coat that falls into the category of nanoscale and their dimensions typically ranges between 20 and 500 of nanometers (10^{-9} m). Significantly, the materials they template also fall into this size range in nanometer scale which has to be found the one can alleviate the cumbersome methodology in nanomaterials synthesis such as size and shape controlled synthesis (Alexandridis, 2011; Wang et al., 2002). Virus capsids are assembled from repeating protein subunits to form highly symmetrical architectures with precise three-dimensional (3D) structure are remarkably stable and in uniform size and shape (Sirotkin et al., 2014; Bothner et al., 1998). The repeating patterns of

amino acid side chains displayed by each protein subunit can function to direct the ordered nucleation of inorganic for the display of novel hybrid molecules on either the interior or exterior surfaces (Flenniken et al., 2009; Klem et al., 2005). Synthesizing nanomaterials via virus entities acting as biological nanofactories offers a clean, nontoxic and environment-friendly method of synthesizing nanomaterials with a wide range of sizes, shapes, compositions, and physicochemical properties (Blum et al., 2004; Sirotkin et al., 2014). In this regard, plant virus nanopatforms lately gathered much attention in the synthesis of metal virus hybrid materials which has many favourable properties like conductance, anisotropy, sensitivity and heterogeneity which can be exploited in a wide range of applications (Steinmetz and Manchester, 2011). For Instance, research revealed that Platinum-metalized TMV particles serve as a building block to fabricate a bio-memory device (Xiao et al., 2013). Living cells can offer ground-breaking solutions to some hard problems faced by the semiconductor industry. Controlled chemical reactions and molecular flows in cells are the ultimate miniaturization of electronics to the atomic and molecular scale (Susmit ang Meghna, 2015). The field of bio-semiconductor is perched for exponential growth. The ongoing miniaturization of bio-semiconductor devices is leading to new opportunities in biomedical research and commercial medical applications. Integration of semiconducting nanomaterials with biological materials has been extensively investigated in various fields. Likewise, the filamentous bacteriophage M13 has been extensively studied as a template for mineralization and has been utilized for semiconductor. Nam et al. (2006), have shown the potential of such an approach in the development of lithium ion battery electrodes using highly ordered M13-templated gold-cobalt oxide nanowires. TMV particles has been employed as a robust functional template for the fabrication of a TMV/zinc oxide field effect transistor (FET) (Sanctis et al., 2015). Likely, there are few examples of electronic devices being directly fabricated from biomaterials owing to a lack of charge transport through them and still, there is much more demand for inorganic-organic hybrid molecules with different and defined geometries for the ideal bio-electronic devices. Therefore, in this investigation, we have exploited a plant pathogenic virus *Squash leaf curl China virus* (SLCCNV) which belongs to *Begomovirus* genus and the family of *Geminiviridae* (Singh et al., 2008; Briddon et al., 1996). *Begomoviruses* are popular known viruses among plant pathologist and almost unfamiliar to the materials science researchers (Scholthof et al., 2011; Varma and Malathi, 2003). The *Squash leaf curl China virus* (SLCCNV) capsid are non-enveloped, about 38 nm in length and 22 nm in diameter, twinned (geminata) incomplete T = 1 icosahedral symmetry capsid that contains 22 pentameric capsomers made of 110 capsid proteins (CP). With this SLCCNV capsid structure, we have been extending its use as a nanofactory or biotemplate for fabricating noble metallic nanoparticles (Au & Ag) without any prior genetic or chemical modification of the exterior surface of virus capsid.

2. Materials and methods

2.1. Chemicals

H₂AuCl₄ (Chloroauric acid) and AgNO₃ (Silver nitrate) were purchased from LobaChemie. Pvt. Ltd. Dialysis membrane

(15 kDa cutoff) and Cesium sulfate (Cs_2SO_4) were purchased from Himedia laboratories, India. Glassware's (Borosil, Scott Duran) and chemicals for buffers and other components for reagents including Uranyl acetate ($\text{UO}_2(\text{CH}_3\text{COO})_2$) and phosphotungstic acid ($\text{H}_3\text{PW}_{12}\text{O}_{40}$) were obtained from Sisco Research Laboratories (SRL), India. For immunoassay, *Begomovirus* coat protein specific *African cassava mosaic virus* (ACMV) TAS-ELISA kit was purchased from DSMZ, Germany. Deionized water (Millipore-18 $\text{m}\Omega\text{ cm}^{-1}$) was used throughout the experiment. All the chemicals were used as supplied without any further purification.

2.2. Virus isolation and purification

The specific symptoms bearing infected leaf samples were collected from the Squash (*Benincasa hispida*-winter melon-*Cucurbitaceae* family) cultivated field near Perambalur district (11.2266°N, 78.9288°E) of Tamilnadu state, India. Among the various host plants, squash varieties are one of the predominant hosts for the *Begomovirus* infections was earlier reported by us (Riyaz et al., 2013). The viral diseases are persistent throughout the year among squash varieties in Tamilnadu state and the rest of the states in India. Thus, there will be no shortage of virions as the biomaterial, even though other *Begomovirus* species sharing the similar structural morphology. The preliminary analysis of the disease was made on the basis of morphological appearance, disease symptoms such as yellowing of vein, leaf curling and the presence of whiteflies on the bottom of the leaves. Collected leaf samples were washed well with Tween-20 at running tap water to remove the dust and other particles then dried and kept in deep freezer further use. The disease pathology in squash plant confirmed by molecular studies, which were already reported in our previous published work (Riyaz et al., 2013). The virus particles or so-called viral templates were purified by Cesium sulfate (Cs_2SO_4) density gradient ultracentrifugation (CP100WX, HITACHI, JAPAN) using fixed angle rotor P100AT2 (803,000g) and swing bucket rotor P55ST2 (366,000g) with necessary modification (Luisoni et al., 1995). The purified virus concentration was quantitatively measured by Enzyme immunoassay (ELISA) (Clark and Adams, 1977). The purity of native virus particles was also confirmed by denaturing gel electrophoresis (Laemmli et al., 1970). Also the virus structure was studied in high resolution transmission electron microscopy (HRTEM) with 2% of Uranyl acetate for negative staining.

2.3. Fabrication of virus-metal-hybrid nanomaterials (Au & Ag)

2.3.1. Preparation of SLCCNV biotemplate

Prior to metal deposition, the purified SLCCNV suspension was dialyzed against different pH buffer (6–11) using 15 kDa cut-off membrane by conventional dialysis method. The virus protein dialyzed against various pH 6–11 buffer (0.1 M phosphate buffer (pH 6–8), 0.1 M sodium borate (pH 9.0), and 0.1 M sodium glycine (pH 10–11)) which gives us the SLCCNV-biotemplate at different pH. By doing so, protein in various pH buffers alters their surface net charge according to their isoelectric point (pI) (Tanford, 1961). The theoretical pI of *Begomovirus* coat protein is reported to be around 10 (Lazarowitz, 1987). Therefore, the net charge of the dialyzed

SLCCNV template was theoretically calculated using the Henderson-Hasselbach equation by web programme (protein calculator v3.4, <http://protecalc.sourceforge.net/>, 2013). The aggregation state of the virus particles which were in different pH also studied in electron microscopy using negative staining.

2.3.2. pH optimization in metal deposition

As a significant step, metal ion deposition was performed using various pH (6–11) buffer dialysed virus template (0.6 mg ml^{-1}). In an Eppendorf tube, a small aliquot of virus template suspensions (100 μl) was taken and mixed with an equivalent volume of 1 mM of gold (Au^{3+}) and silver precursor (Ag^{2+}) solutions as well. After two minutes gentle vortexing, the reaction suspensions were kept in direct bright sunlight ($\sim 40^\circ\text{C}$ Max) to induce the photocatalytic reduction for at least 5–10 min (Eustis et al., 2005). The reaction mixtures were monitored till the visible colour change (wine red and yellow) which might be indicated in the synthesis of gold and silver nanomaterials respectively. After the visible colour change if any, the reaction suspensions were taken to the shadow place to stop the reaction. Both Au and Ag reaction suspensions were subjected to the further evaluation and characterization.

2.3.3. Concentration optimization in metal deposition

Two steps were optimized for nanomaterials fabrication on SLCCNV, likely the ratio of mixing concentration between the virus protein and precursor ions (Au^{3+} & Ag^{2+}). Based on the obtained results from pH optimization, here we have been utilizing pH 10.0 buffer dialysed SLCCNV-template alone for this study. The first reaction was carried out by mixing the standard volume containing (0.6 mg ml^{-1} , 100 μl) SLCCNV-biotemplate with a diverse volume containing 1 mM concentration of precursor ions (Au & Ag) at the ratio of 1:0.5, 1:1, 1:1.5, 1:2, 1:2.5 and 1:3. Followed that next reaction was carried out by mixing standard volume containing 1 mM precursor concentration (Au & Ag) with the various volumes of SLCCNV-biotemplate suspensions at the ratio of 1:0.5, 1:1, 1:1.5, 1:2, 1:2.5 and 1:3. After that, all reaction suspensions were stirred gently and then reaction tubes were kept in direct sunlight for at least 5–10 min for the visible colour change. The outcome of this parameter has timely monitored and recorded by UV-Vis spectrophotometric analysis.

2.4. Physicochemical characterization

2.4.1. Spectroscopic analysis

After fabrication process, all the resultant samples in the form of suspensions were collected periodically during the experiment to monitor the reduction nucleation of noble metal precursor ions at the surface of SLCCNV, followed by the dilution of samples with 2 ml of deionized water and subsequently scanned for UV-Visible spectra, between the wavelengths of 200 to >1000 nm (UV-1601 spectrophotometer, Shimadzu, Japan) with UV probe 2.33 version software. The absorbance was recorded and plotted by absorbance at Y axis and wavelengths in nm in the X-axis. In addition, the same UV-Vis spectrometer used to study the temperature stability of fabricated virus-metallic hybrid nanomaterials. However, thermal stability is one the significant physical factor which can influence nanomaterials stability when it's comes to application towards electronic devices. Therefore, it was taken into

the account of characterization, where SLCCNV fabricated nanomaterial was incubated at UV-Vis spectral instrument. To know the hydrodynamic size of the virus fabricated samples, it was measured using dynamic light scattering (DLS) spectroscopy system (Photocor Instruments) that was equipped with a 20 mW He-Ne laser ($\lambda = 632 \text{ nm}$). DLS measurements were taken at a 90° scattering angle. Surface Enhanced Raman Scattering (SERS) also conducted to identify the surface amino acid residues which act as nucleation sites over virus particles. SERS is a highly sensitive technique that provides enhanced Raman signal of vibrational information specific to the chemical bonds and symmetry of molecules (Han et al., 2009). For SERS analysis, samples were pelleted and coated on the ethanol washed the glass and kept vacuum dry for 30 min. From SERS, differential vibrational peaks were observed for both virus-metallic-hybrid nanomaterials (Au & Ag) and documented.

2.4.2. Electron microscopic analysis

The ultra fine surface topology of SLCCNV fabricated nanomaterials was determined by Field emission scanning electron microscopy (FESEM, Hitachi, SU-6600) with an accelerating voltage of 30 kV. Samples were mounted on a piece of copper plate (1 cm^2) then air-dried to analysis at FESEM. The ultrafine cross-sectioned electron images of SLCCNV-metal-hybrid nanomaterials were obtained from HRTEM-FEI, TechnaiG2, 30S-TWIN D905, USA. Specimen samples ($2 \mu\text{l}$) were dropped on a carbon coated copper grid (EM grids, 300 mesh, Sigma-Aldrich) and dried in air at RT. Then, the copper grid was placed in the sample holder and HR-TEM operated at an accelerating voltage of 200 kV with a high-resolution pole piece, lattice images were recorded. Subsequently, both Energy-dispersive X-ray spectroscopy (EDX) and Selected area electron diffraction (SAED) were taken by the same HRTEM instrument to confirm the molecular composition and crystalline nature of fabricated SLCCNV-metal hybrid nanomaterials (Raja muthuramalingam et al., 2015, 2016). The particle size distribution of metal nanomaterial over the surface of SLCCNV were analysed through obtained HRTEM micrographs using ImageJ 1.5 software (Schneider et al., 2012).

2.5. Biocompatibility of SLCCNV-metallic-hybrid nanomaterial

While developing a novel nanomaterials for biomedical application, an essential criterion that needs to be tested prior to contact with the mammalian system is whether they are non-cytotoxic or biocompatible. Thus, here biocompatibility properties of both Virus-metallic-hybrid nanomaterial (Au & Ag) along with virus particles were determined in a concentration-dependent manner by an MTT assay in A549 lung cancer cell line (Satish et al., 2009). This colorimetric assay is based on the ability of cellular mitochondrial enzymes (Succinate dehydrogenase) to reduce the yellow water-soluble substrate 3-(4,5-dimethylthiazol-2-yl)-2,5-diphenyl tetrazolium bromide (MTT) to an insoluble dark purple coloured formazan crystals. Reduction of MTT dye can only take place in metabolically active cells and the level of activity is a measure of the viability of the cells (Mosman, 1983; Wilson, 2000). The resulting formazan crystal was dissolved in 100 μl

of DMSO (Dimethyl sulfoxide) with gentle shaking and the absorbance was measured at 595 nm using an ELISA reader (BioTek power wave XS, USA), all experiments was carried out in three times independently and the average of all experiments has been shown as a cell viability percentage in comparison with the control experiments, while untreated controls were considered as 100% viable.

$$\text{Cytotoxicity \%} = [1 - (\text{OD}_{\text{treated}}/\text{OD}_{\text{control}})] * 100$$

where $\text{OD}_{\text{treated}}$ and $\text{OD}_{\text{control}}$ corresponded to the optical densities of treated and control cells. The rate of cytotoxicity calculated from the absorbance values that are lower than the control cells indicates the percentage of cell proliferation. The percentage of cytotoxicity or biocompatibility (%) plotted against a function of concentration.

2.6. Electrical conductivity analysis

A device was ingeniously made by us with simple available materials to check the electrical conductivity (EC) of the fabricated SLCCNV-metallic-hybrid nanomaterials (Fig. S1, Supplementary data). A prime component has built up with a replaceable glass slide (3.75 mm^2) on the top of the device which is for sample loader. Two copper plates (electrodes) were placed at the edges (face to face) of a glass substrate which was interconnected with battery (2V) and a small LED bulb (1.5 V) directly. However, LED bulb was connected directly to one electrode to recognize the conductivity of testing material visually (glow or dim) when it loaded between the two electrodes over the glass substrate. A fixed volume ($10 \mu\text{l}$) of pH 10.0 fabricated SLCCNV-metal-hybrid nanomaterial (Au & Ag) suspensions with control SLCCNV protein were separately coated onto glass substrates ($\sim 1\text{-}\mu\text{m}$ thickness) to acquire a conductive pattern using the micropipette technique. After complete dehydration (at 45°C) of coated samples, the glass substrate was placed between electrodes. The ability of the testing nanomaterial to transport the electrical charge was confirmed by the glow of the LED bulb as soon as the glass substrate contact the electrode. The same glass substrates coated with hybrid nanomaterials and virus protein used for current-voltage (IV) measurements using Keithley 6487 voltage source meter. For an applied potential corresponding current was measured using a pico-ammeter (0.1–1 Volts). The resistance of the samples was determined from the slope of the linear fit of I-V plot ($R = V/I$).

Supplementary data associated with this article can be found, in the online version, at <https://doi.org/10.1016/j.arabjc.2018.07.006>.

Using the relation

$$\rho = RA/l, \quad \sigma = 1/\rho$$

the conductivity of the samples were calculated where

ρ is the resistivity of the samples (mho)

R is the electrical resistance of the sample ($\Omega\text{-m}$)

A is the cross-sectional area of glass substrate ($l \times b$) (m^2)

l is the thickness of the samples coated on glass substrate (μm)

σ is the conductivity of the sample (Siemens/metre)

3. Results

Caesium sulphate gradient ultracentrifugation yields a good quantity of SLCCNV particles (0.6 mg ml^{-1}) with homogeneity which is determined by a single intensified protein band in the silver stained SDS-PAGE gel (see Fig. S2). However, a single protein band directly denotes that the virus particles retained its capsid structure against optimum denaturing temperature, which justifies them as an obligate microorganism and its prevailing capsid integrity. In making of SLCCNV particles as a biotemplate, dialysis with different pH buffer produced the SLCCNV-biotemplate suspensions to its respective pH. It has been confirmed by simple pH analysis. Then it was assumed that all the dialysis underwent SLCCNV particles were electronically active to their respective buffer pH strength along with a customized surface net charge. Fig. S3, shown the theoretically calculated (Henderson-Hassel Bach equation) net charge values of SLCCNV-biotemplate dialyzed against different pH parameters. However, the net charge on a virus protein is zero at the isoelectric point (pI), positive at pHs (6, 7, 8 & -9) below the pI, and negative at pHs (11) above the pI. The net charge on a protein at any given pH is determined by the pKa values of the ionizable groups. The virus particles in the pH of 7–10 remain stable in their shape and structure which was observed in negative staining under electron microscopy (data not shown).

3.1. Fabrication of SLCCNV-metallic-hybrid noble nanomaterials

The pH (6–11) altered and activated viral template was effectively reduced both precursor ions (Au & Ag) and form SLCCNV-metallic-hybrid noble nanomaterials. It was determined after the visible colour change of both gold and silver reaction solution kept in the direct sunlight about 5–6 min. The reaction carried out at least for five replications and then determined. Notably, among other reaction solution, only

one reaction solution ends up with bright colours, that was observed in the pH 10 virus template. Certainly, it was a direct indication of nanoparticles synthesis with the perfect geometries. Remaining reaction solution were varied in their colour exhibition from purple to pink. The pH 10 virus template fabricated nanomaterials have got their standard UV–visible spectrum peak at 540 nm and 420 nm for both gold and silver respectively (see Fig. 1 A & B). The colour indication corroborates to the surface plasmon resonance (SPR). This signifies that “when the dimensions of a metal is reduced to the nanoscale, the optical properties are dominated by an oscillation of conduction of electrons in resonance with incident electromagnetic radiation”. Every colloidal metal nanoparticles have its own SPR and colours. Moreover, we have observed different colour (Gray to Red for Gold & Pale yellow to brown for silver) formation of reaction solution from pH 6 to 11 which may indicate the gradual synthesis of nanomaterials in the solution (Pratibha, 2009). These colour changes can be ascribed to the size and shape of NPs in the suspensions. The size variation of smaller to larger particles in the solution would apparently shows in the colour intensity (SPR) to light to dark. The absorbance peak (λ_{max}) of both nanomaterials had shown gradual variations which directly attribute to the growth of the nanoparticles over pH altered SLCCNV template (see Fig. 1 A & B). In another experiment, optimized concentrations of both precursor and viral biotemplate produced the ideal hybrid virus nanomaterials (Au & Ag) that were primarily investigated by UV–Vis absorbance peak (λ_{max}) at 420 nm and 520 nm for silver and gold respectively. As outlined in Fig. 2(A, B, C & -D), the UV–Vis spectral data clearly shown that the concentration of both precursors (Au & Ag) and virus biotemplate systematically played very well for the fabrication of hybrid nanomaterials. However, when precursor concentrations (Au & Ag) was high and virus template concentration was low (3:1), the corresponding absorbance peak (λ_{max}) was shifted to broad in the wavelength indicates that both gold and silver nanoparticles are bigger in size. Similarly, while the virus template concentration was high, whereas the precursor

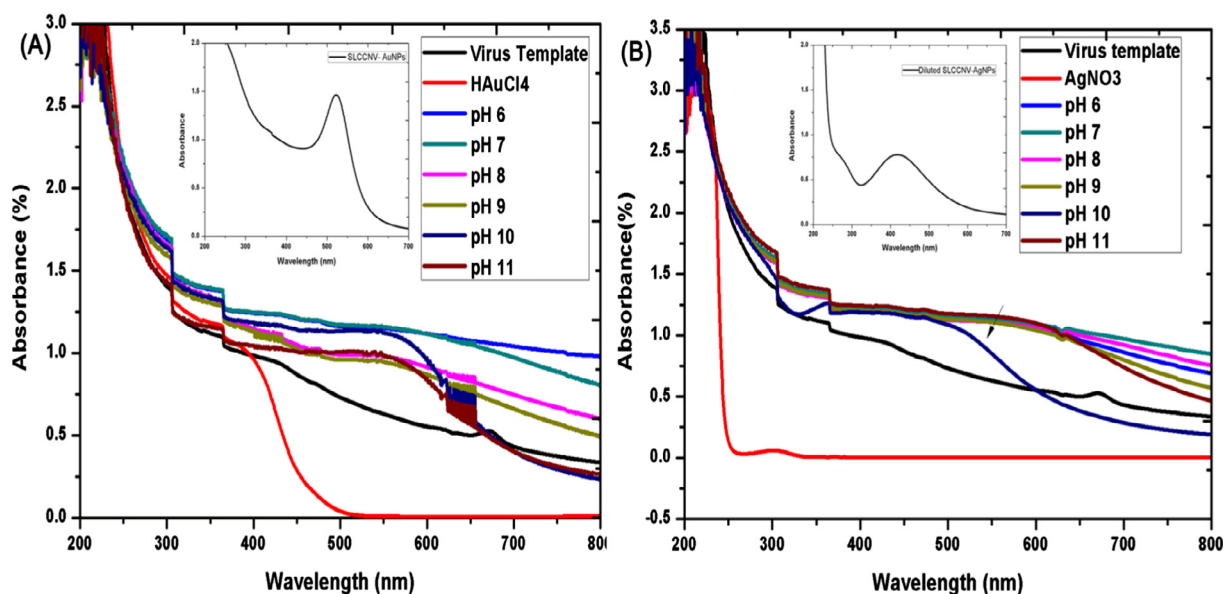


Fig. 1 UV/Vis absorbance spectrum of pH-activated-SLCCNV-biotemplate mediated fabrication of nanomaterials with gold (A) and silver (B) precursors. A & B (Inset) shows the absorbance spectrum of one time DDH₂O diluted pH 10-virus hybrid nanomaterial.

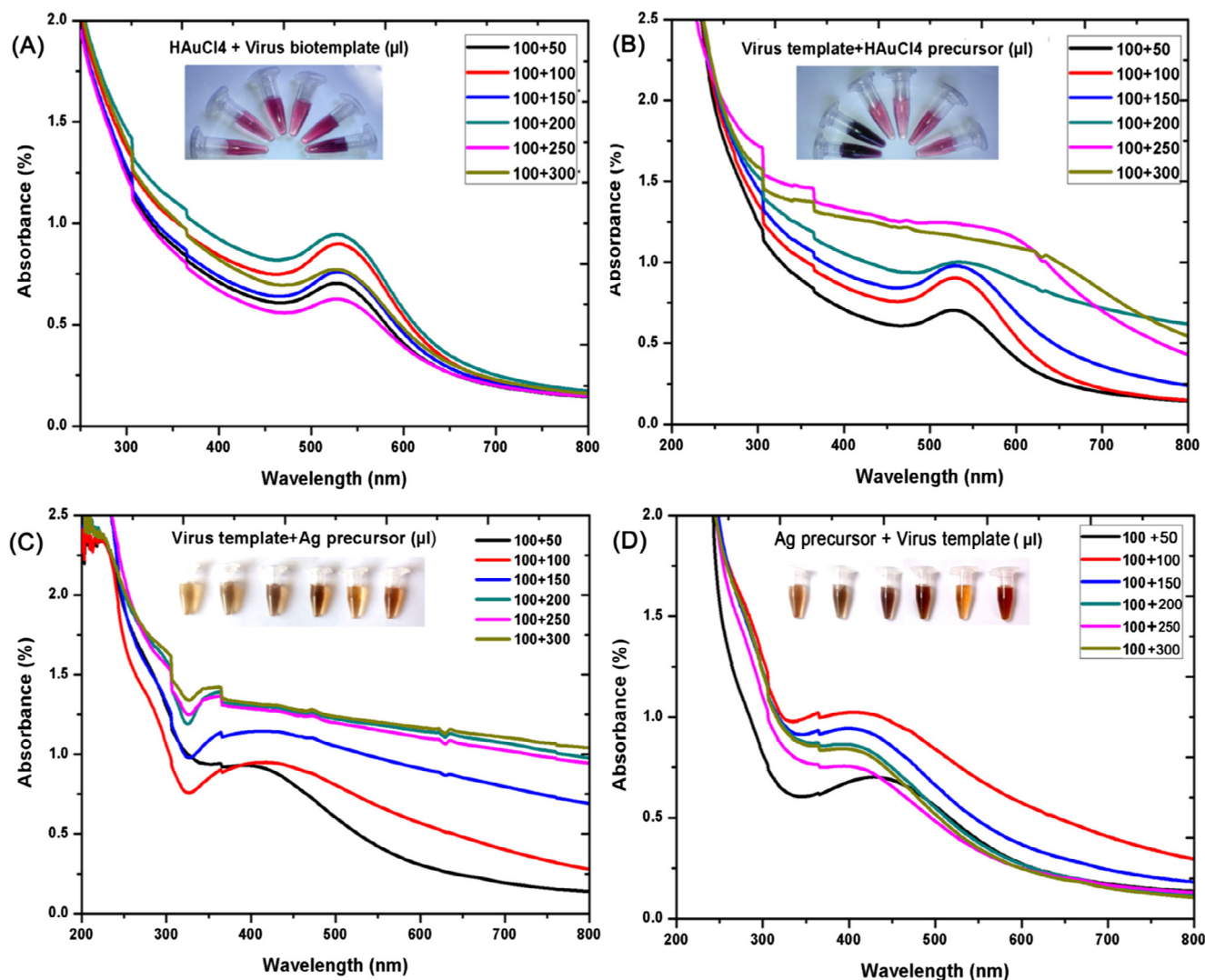


Fig. 2 UV/Vis absorbance spectrum of concentration dependent fabrication of virus hybrid nanomaterial – (A–D); Different ratio of virus template and (Au & Ag) metal ion precursor. Graphs shows the two reaction conditions like standard concentration of virus template with the various concentration of (Ag & Au) precursors (B and C) and secondly, standard concentration of precursors with the various concentration of virus template (A and D).

concentration was low (3:1), the UV absorbance peak (λ_{max}) were shifted to sharp at the corresponding wavelength of both gold (~ 520 nm) and silver (~ 420 nm) which indicated that fabricated metal nanomaterials was in smaller size. At the same Fig. 2(A, B, C & –D), the maximum absorbance peak (λ_{max}) at 520 nm (gold) and 420 nm (silver) was observed for the combination of equal concentrations (1:1) of both virus templates and precursor. It apparently shows that, only equal concentrations (1:1) have yield defined nanomaterials with homogenous sized particles which was assumed by the previous study of characteristic absorption spectrum for both gold and silver nanomaterials (Wolfgang et al., 2007; Alvin et al., 2015).

3.2. Characteristic features of SLCCNV-metallic-hybrid nanomaterials (Au & Ag)

3.2.1. Thermostability analysis by UV–Vis spectra

In this study, pH 10 virus template fabricated metal nanomaterials were subjected to thermostability analysis in a colloidal

condition at various temperatures. Fig. S4, shows the UV–Vis absorption spectra of hybrid nanomaterials (Au & Ag) which forecasting that particles were responded differently to the temperature variation. However, at 20 °C, 35 °C, 40 °C and 45 °C there was an apparent shift of the absorption maximum (λ_{max}) at 500 nm–650 nm which regards the progressive particle aggregation only in virus-gold hybrid nanomaterials (see Fig. S4, A). Temperature above 45 °C, the hybrid AuNPs had shown characteristic absorption peak at 520 nm which indicated the stability of the materials even up to 55 °C (see Fig. S4, A). Whereas, in the case of hybrid AgNPs, it showed noticeable aggregation only at 40 °C and 45 °C as the gradual shift of longer wavelength in absorption spectra at 400 nm–500 nm (see Fig. S4, B). Incubated below 40 °C and above 45 °C shows excellent stability in hybrid AgNPs which reached its characteristic absorption maximum at 420 nm. Significantly, temperature at 55 °C, the hybrid AgNPs shows superior thermostability than hybrid AuNPs (see Fig. S4, A & B).

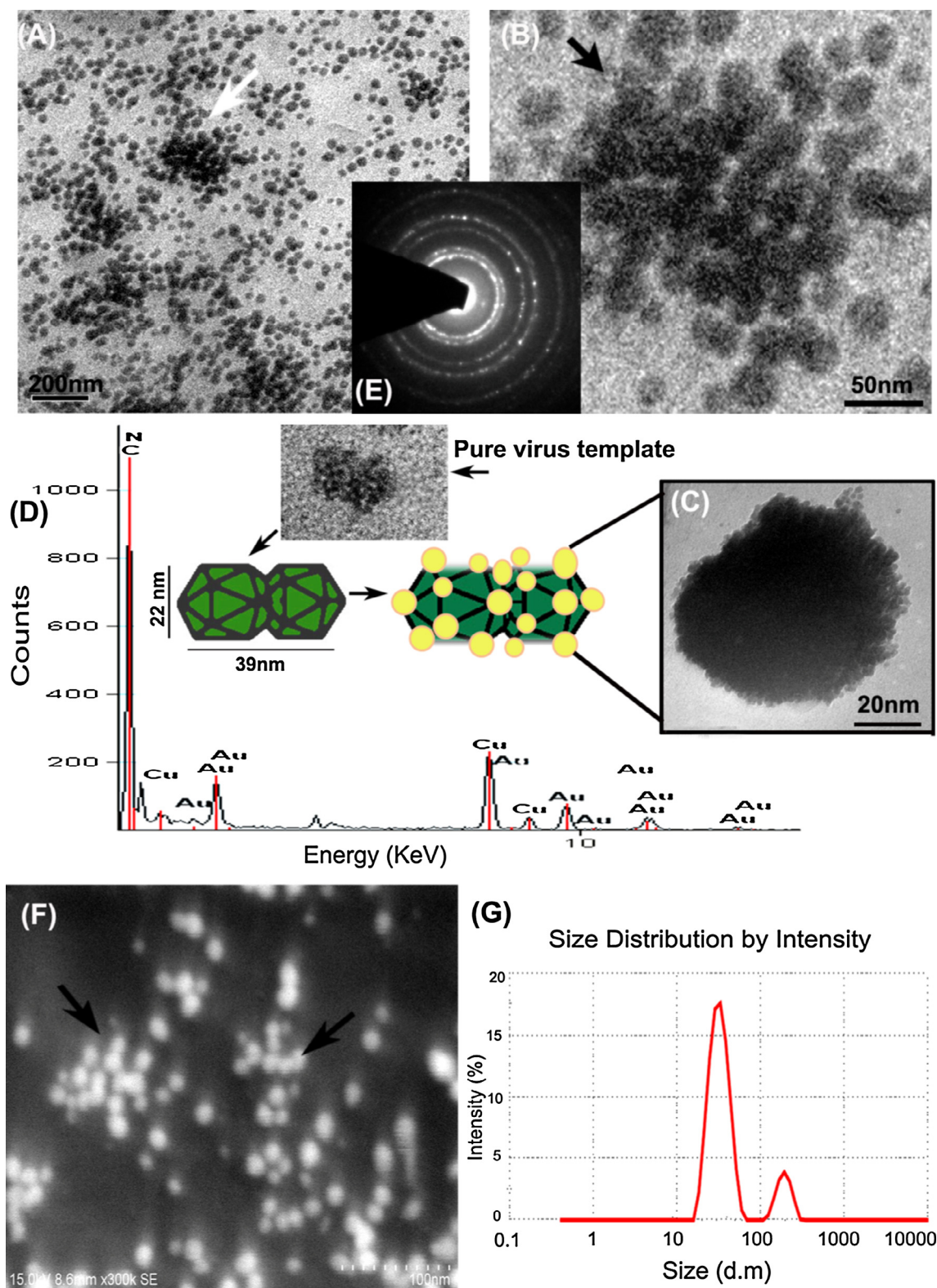


Fig. 3 All images corresponding to virus fabricated hybrid gold nanomaterials (A)–(C) HRTEM images taken in various nanoscale bars such as 100 nm, 50 nm and 20 nm shows the virus particles decorated with a densely packed array of gold nanoparticles (D) EDX spectra representing the molecular species, (E) SAED diffraction pattern (F) FESEM image (G) DLS spectrum of hybrid AuNPs. Inset showing pure virus particles with similar graphical representation.

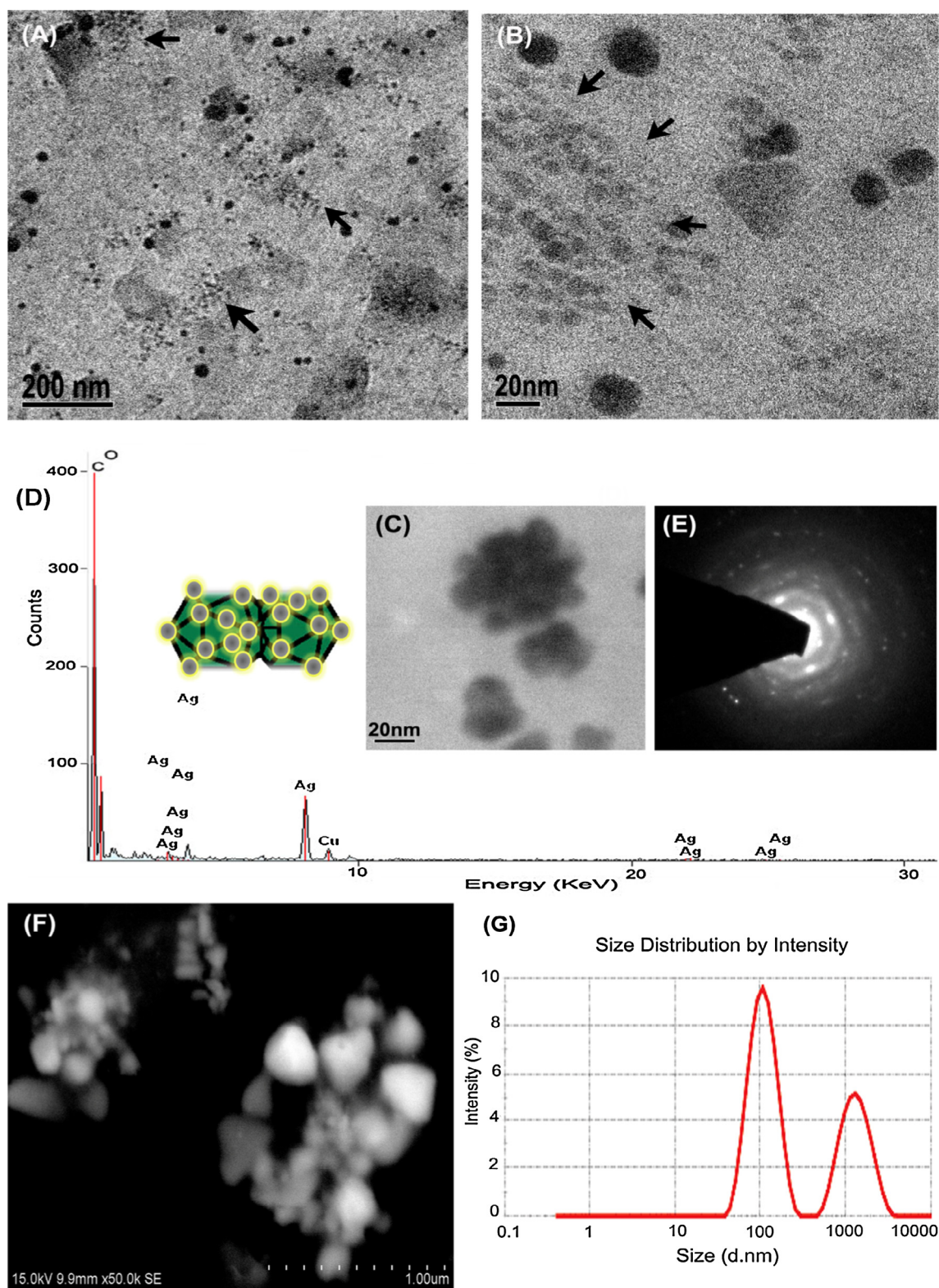


Fig. 4 All images corresponding to virus fabricated hybrid silver nanomaterials (A)–(C) HRTEM images taken in various nanoscale bars such as 100 nm, 50 nm and 20 nm shows virus particles decorated with a densely packed array of silver nanoparticles (D) EDX spectra representing the molecular species, (E) SAED diffraction pattern, (F) FESEM image and (G) DLS spectrum of hybrid AgNPs.

3.2.2. Electron microscopy and DLS analysis

With the aid of electron microscopy, the topology of fabricated virus-metal-hybrid nanomaterials was closely studied (Cao et al., 2011). Very interesting features were found in HRTEM images taken at 100 nm and 50 nm scale. However, Figs. 3 and 4A and B, electron image shown the number of gold and silver nanoparticles uniformly decorated around the viral capsid may resemble the islands of nanoparticle clusters. Similarly, electron images taken at 20 nm scale have evidently shown how majestically a single virus particle decorated with nanoparticles through surface mineralization over their entire capsid surface (see Figs. 3 and 4C). FESEM observation at 100 nm magnification also correlated with the similar morpho-

logical features seen in HRTEM images for both hybrid nanomaterials (see Figs. 3 and 4F). The FESEM image is a distinct evidence of surface mineralization capabilities of SLCCNV. From obtained electron images, we could have roughly determined the sizes of the both Au & Ag nanoparticles decorated over the virus capsid is 5–12 nm and 5–20 nm respectively. Though, the accurate size of the nanoparticles distributed over the virus capsid was determined through processing the HRTEM images of ImageJ software (video tutorials also available on YouTube). As shown Fig. 5A and B (inset), histogram represents the size distribution of nanoparticles around the virus capsid summarized by analyzing the corresponding TEM images of gold and silver nanoparticles. It was

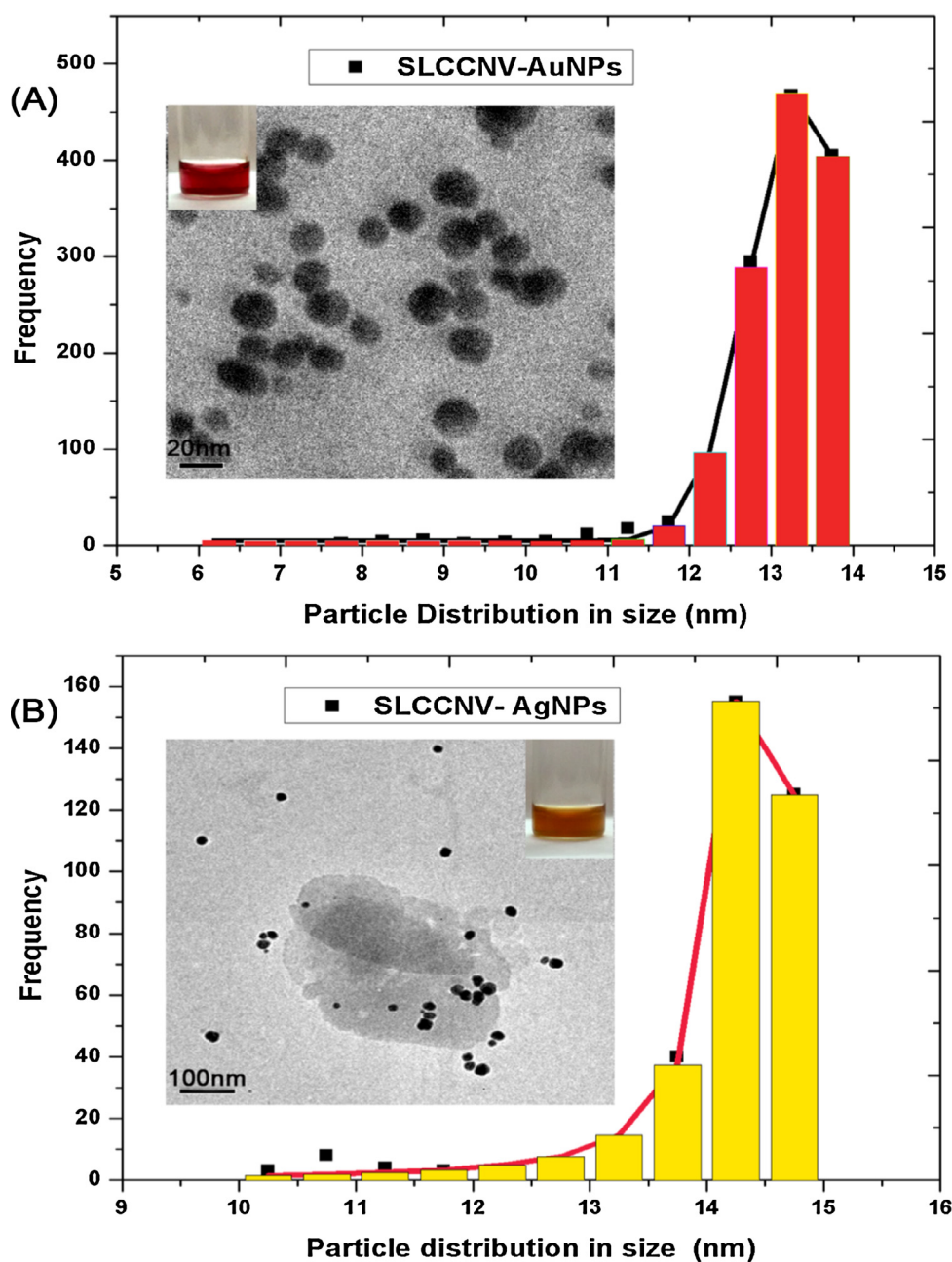


Fig. 5 Histogram showing the particle size distribution corresponding to the HRTEM images of (A) Virus hybrid gold nanomaterial and (B) Virus hybrid silver nanomaterial.

determined that gold nanoparticles have size ranges between 6 and 14 nm in diameter and silver nanoparticles contain particle size ranges between 10 and 15 nm. Also, a higher number of standard sized particles (~ 14 nm) were also detected in the histogram (see Fig. 5A and B).

Next Figs. 3 and 4G, the DLS spectroscopic data, we were detected two species in the colloidal medium likely to be individual virus-metallic-hybrid nanomaterial and nanoparticles detached from the virus template. However, a hydrodynamic size of the two species in the medium was varied between gold and silver. Apart from the nanoparticles size already mentioned, the size of the individual both gold and silver virus-metallic-hybrid nanomaterials were determined between 50 and 300 nm and 300–1100 nm respectively. Indeed, the virus particle size has exponentially increased by offering nucleation sites for metal precursor in which nucleation cropped up over the virus, possibly increases the size upon the precursor concentration in the medium. In Figs. 3 and 4D displays an EDX (Energy dispersive X-ray spectroscopy) elemental analysis map which shows the spectrum containing abundant gold and silver elements along with C, N environment confirmed the presence of proteinaceous groups gives higher counts in the map. Especially, there was no other contamination detected in the EDX spectrum, which demonstrates the purity of virus-metallic-hybrid nanomaterials.

The diffraction pattern obtained through SAED had shown peculiar features for hybrid AgNPs. As seen in Fig. 4E, the SAED pattern shows the crystalline orientation in bright spots that resembles the icosahedral ($T = 1$) symmetry of *Squash leaf curl China virus* capsid. In the same Fig. 4E, it is visible that the small spots of a polycrystalline pattern of the silver nanoparticle arise from the core virus crystallite. In Fig. 4E, the SAED pattern corresponding to the hybrid AuNPs had shown the polycrystalline nature (arranged in regular three-dimensional lattices) of the virus and its associated gold nanoparticles. In particular, nucleation sites present in the virus capsid transformed their amorphous phase to crystalline phase through the nanofabrication process by the nucleated noble nanomaterials.

3.2.3. Surface Enhanced Raman spectroscopy

SERS allows us to predict the single molecule attachments on virus particles utilized for nanofabrication. In this analysis, three different vibrational excitation spectra corresponding to the reference SLCCNV and two virus-metallic-hybrid nanomaterials was recorded. Fig. 6 A shows a characteristic SER spectrum (A) taken for SLCCNV, vibration peaks are due to Amide I band 80% C=O stretch, near 1650 cm^{-1} , Amide II band 60% N-H bend and 40% C-N stretch, near 1550 cm^{-1} , Amide III band 40% C-N stretch, 30% N-H bend, near 1300 cm^{-1} . Near 702 cm^{-1} denoted for tryptophan amino acid and near 1000 cm^{-1} intense band for phenylalanine amino acid (Xu et al., 2014). Fig. 6B & C shows typical SER spectra of hybrid nanomaterials, clearly demonstrated that the silver and gold nanoparticles exhibit its originations from the virus proteins. However, comparing the spectrum of SLCCNV, there is quite sensitive relevance observed in the Raman intensity peak, which demonstrates the possibility deprotonation of amino acid (of SLCCNV) between 1000 cm^{-1} to and 1550 cm^{-1} by the formation of both nanoparticles. On the Spectra of Fig. 6B & C, the vibrational energy

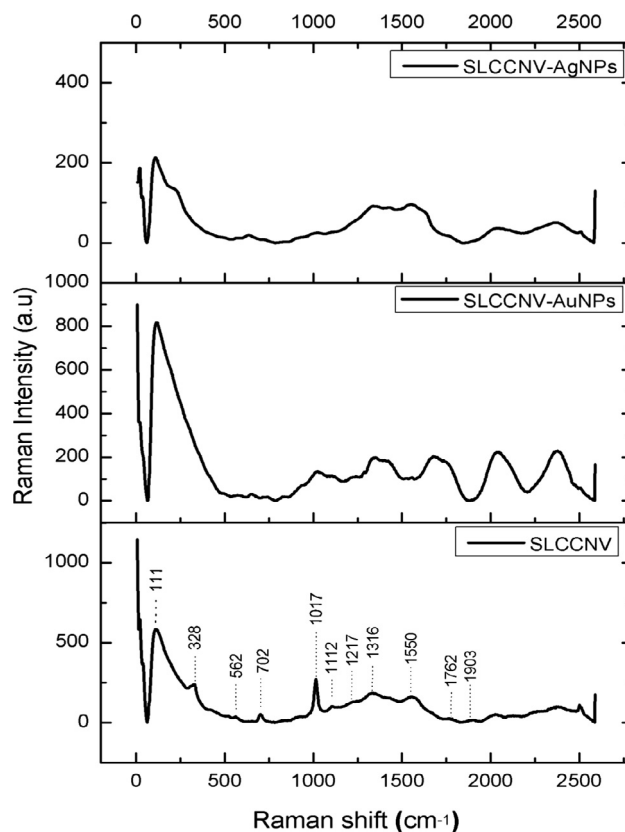


Fig. 6 SERS spectra from pure SLCCNV protein, SLCCNV fabricated gold nanomaterial and SLCCNV fabricated silver nanomaterial. Characteristic Raman shifts are indicated by the wave number.

is little higher in gold nanoparticles than silver nanoparticles. Apparently, new bands detected in spectrum B with longer wavelength 1550 cm^{-1} to 2400 cm^{-1} corresponds to the gold atom (Seongmin and Xiao, 2013). Whereas in the case of silver nanoparticles, there is no enough vibrational peak detected at 1350 cm^{-1} stretch which is a strong characteristic resonance peak for silver atom (Watanabe et al., 2005). It is also important to note that all the Raman scattering frequency were obtained in low intensity due to the availability of virus protein and associated nanoparticles (Kevin and Juan, 2011). This similar phenomena was already reported by Segnan et al. (2009). In his report, the incident laser light will produce autofluorescence at biomaterials, which is usually much more intense than the Raman scattered light. This fluorescence can make the Raman signals difficult or even impossible to measure.

3.3. Biocompatibility of SLCCNV-metallic-hybrid nanomaterial

Since the MTT assay is a colorimetric assay, the reduction of MTT in viable cells treated with reference SLCCNV and two SLCCNV fabricated hybrid nanomaterials were measured at 595 nm, the data shown in Fig. 7. The cytotoxicity profile of a plant virus shows good biocompatibility features at all the eleven ($10\text{--}110\text{ }\mu\text{l}$) concentrations (multiple of $600\text{ }\mu\text{g}/\mu\text{l} \times 11$). Whereas SLCCNV fabricated hybrid nanomaterials treated cells shows reduced viability (70%) up to the concentrations of $90\text{ }\mu\text{l}$. Further, the cell viability outreached the cytotoxicity

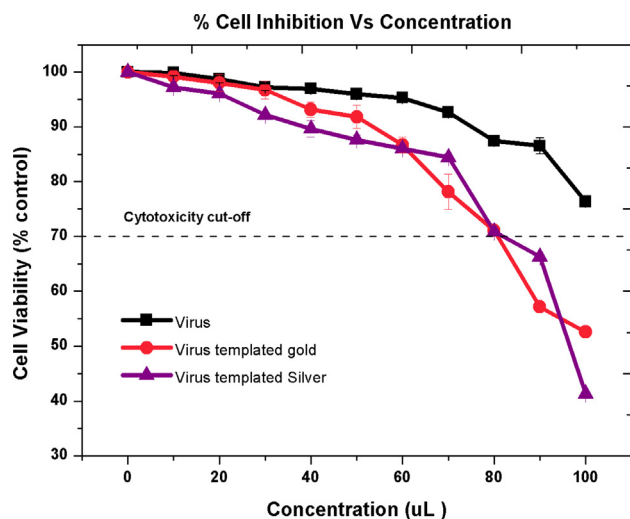


Fig. 7 Cytotoxic effect of SLCCNV protein, SLCCNV fabricated gold nanomaterial and SLCCNV fabricated silver nanomaterial on the A549 lung cancer cell line measured by the MTT assay. The percentage of cytotoxicity or biocompatibility (%) plotted against a function of concentration. Data are shown as SD with SE for three different experiments. The line represents the fit to the experimental data points.

cut off range of the concentrations exceeds at $< 90 \mu\text{l}$ for both hybrid nanomaterials. In comparison with silver nanomaterials, gold has shown ample better biocompatible features up to $50 \mu\text{l}$ ($> 90\%$).

3.4. Electrical conductivity of SLCCNV-metallic-hybrid nanomaterials

Both gold and silver hybrid nanomaterials visually confirm its ability to conduct the electrical charge by the glow of the

LED bulb as soon as the nanomaterials coated glass substrate contact the electrode (see Fig. S1). Surprisingly, the purified virus protein has shown EC properties resulting in the glow of the bulb. Through pico-ammeter, we have obtained a solid evidence of conductivity for all three samples by measuring the resistance of samples at a different voltage. In Fig. 8A illustrates the resistance (ohm) of samples and Fig. 8B a histogram illustrates the conductivity (mS/m) of samples which was calculated from the resistance of samples using by Ohm's law. Only virus hybrid nanomaterials showed resistance properties at the input of voltage (V) from 0.1 to 1 (see Fig. 8A). The pure virus protein shows almost Zero resistance properties at the input of various voltage which means it showed good conductive properties. In the same Fig. 8A, both virus hybrid nanomaterials similarly maintain its resistance in a steady state against the application of an external voltage. Presumably, the hybrid materials will show standard resistance properties and stability against the higher electrical field. As a result, pure virus protein exhibit very low and no resistance properties, whereas hybrid nanomaterials have shown moderate resistance properties. The determination of electrical conductivity (EC) of samples is directly reciprocal of the resistance of the samples. Therefore, there might be an increased conductivity of the samples when there is the increased voltage (V). By the result of electrical conductivity equation (Ohm's law), it was determined that pure SLCCNV protein has elevated conductivity properties (0.031 mS/m) than the other two fabricated nanomaterials. It was 0.006 mS/m ($6 \times 10^{-5} \text{ S/cm}$) for hybrid AgNPs and 0.009 mS/m ($9 \times 10^{-5} \text{ S/cm}$) for hybrid AuNPs. Since the optimal semiconductivity lies between the band gap of 10^{-6} to 10^{-2} we have achieved a good bio semiconductor material.

4. Discussion

The destructive plant pathogenic virus of *Squash leaf curl China virus* presents a confined environment and unique twin

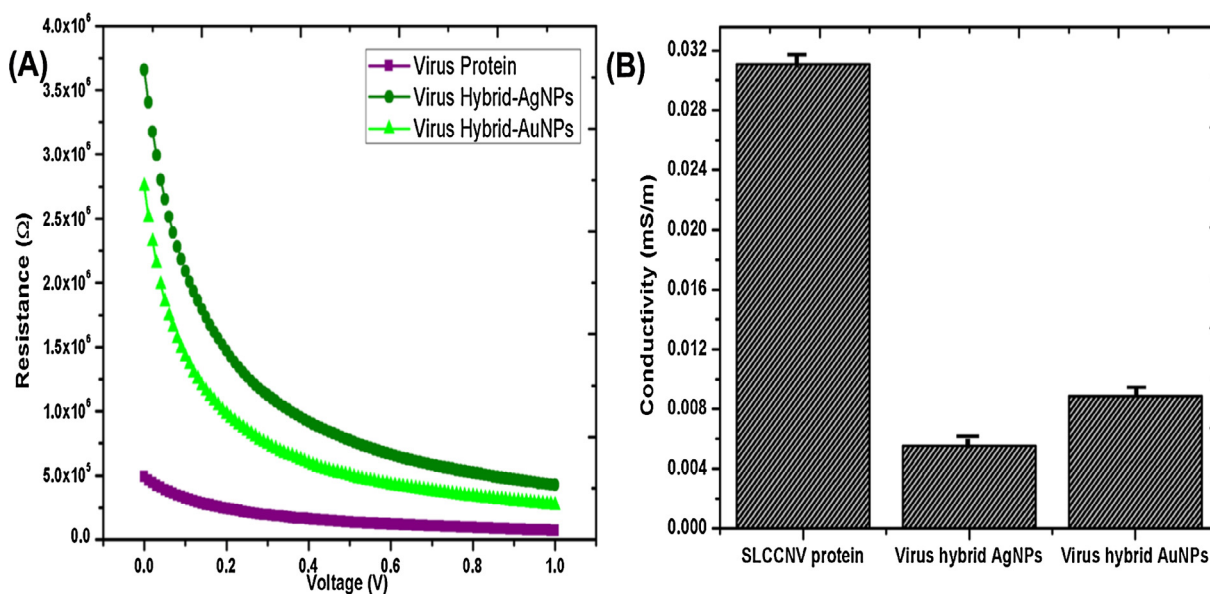


Fig. 8 Electrical conductivity (EC) analysis of SLCCNV protein, SLCCNV fabricated gold nanomaterial and SLCCNV fabricated silver nanomaterial, (A) Pico-ammeter measured materials resistance properties at various voltage sources (0.1–1 V), (B) Histogram represents the electrical conductivity of materials (Data are shown as standard deviation with error bar).

icosahedral protein surface topology for noble metallic nanoparticle synthesis and are amenable to nanotechnology manipulations. The metal deposition on SLCCNV has successfully produced the SLCCNV-metallic-hybrid noble nanomaterials at optimized condition related to the ionic strength of virus template and the concentration of both template and precursor ions. In the first approach, the SLCCNV capsid actively potentiated the reduction of both Au and Ag metal precursors by protonation from electronically activated solvent exposed amino acid residues resulting into the virus-metallic hybrid nanomaterials (AuNPs and AgNPs). It was found that viral reduction appeared to be selective for noble metals like gold and silver and the similar work was reported using *Tobacco mosaic virus* earlier by Bromely et al. (2008) and Dujardin et al. (2003). We are absolutely agree with the another report stated that the preparation of virus templates with altered surface charge by pH is certainly a significant guiding factor for nanofabrication process (Namba and Stubbs, 1986). When the pH (10) conditions were adjusted equal to the isoelectric point of virus protein, produced a highly reactive amino acid functional groups rendered a successful nanofabrication, also evidenced by previous work (Balci et al., 2006; Knez et al., 2004). Amino acids are highly reactive in its native conditions (Tan et al., 2010). Therefore, metal ion binding possibly occur via N-terminal amino and C-terminal carbonyl groups, or through side chains such as the ring nitrogen atom of histidine, or the carboxylate groups of aspartic and glutamic acid. Moreover, metal ion reduction may be facilitated by hydroxyl groups in tyrosine and carboxyl groups in asparagine and glutamine, and indole groups on tryptophan (Tan et al., 2010). All 20 amino acids have their pI (Isoelectric point) and pKa values (the acid ionization constant of a solution) determined by the pH of the medium in which the protein exists. In our case, we are not certain about what type of amino acids involved in the surface mineralization process. However, it can be determined by the pH-dependent characteristics of the virus protein and its pKa values, where $\text{pH} = \text{pI}$ (the number of negative and positive charge is equal). Following the same phenomenon, we have used pH 10 buffer dialyzed viral protein as a template for surface mineralization. The pH-activated virus template at their neutral charge facilitates a highly reactive nucleation sites (primary COO^-) which could draw charged metal ions (Au^+ and Ag^+) to initiate the mineralization process and that point of time are called as nucleation point (Douglas and Young, 1998; Dujardin et al., 2003). After the initial nucleation, more precursor ions in the reaction solution electrostatically drive to the nucleation site to further growth of nanoparticles over the virus template (Nguyen et al., 2014). Reduction of the gold precursor at the virus template produced the colloidal suspension in wine red colour with the characteristic absorbance spectra near 520 nm and reduction of silver precursor produced a yellow coloured colloidal suspension with absorbance spectra near 420 nm. Both gold and silver virus hybrid nanomaterials were fabricated within 5–10 min of exposure to direct sunlight. At the time, the concentration factor also plays a significant role in this nanomaterial fabrication (Chandran et al., 2006; Monaliben et al., 2015) where evidenced by UV-Vis absorption spectra, DLS and nanoparticles size distribution analysis by ImageJ (see Figs. 2, 3G, 4G and 5). As a result, it produced a narrow size distribution during a metal deposition over virus templates. Where the lower concentration of precursors produced smaller particles

and higher concentration produced larger ones. Similarly, low concentration of viral template offers a minimum number of nucleation sites and a higher concentration of viral template offer a higher number of nucleation sites where possibly produce the homogenous size nanoparticle by adjusting the precursor concentration. An important feature perceived in all electron microscopy images is all nanoparticles seems to be unconnected to each other with sub-nanometer scale distances (Figs. 3 and 4). Basically, the virus capsid has well defined structural symmetry with multiple protein subunits. Every subunit in the capsid is eligible to act as a biotemplate for nanoparticle synthesis. Therefore a single virus can act as a “nanofactory” to synthesis ‘n’ number of particles with a defined size. Figs. 3 and 4F FESEM images also reveal the shape of the nanoparticles such as gold nanoparticles are observed in truncated octahedron (sphere) shape, whereas silver nanoparticle was found to have anisotropic nanostructures like truncated octahedron and tetrahedron (Pedro et al., 2015). The EDX observations confirm the presence of virus protein and associated metal precursor in the pure form. It also suggested that there are no other elements involved in the hybrid nanomaterials fabrication (Figs. 3 and 4D). SAED diffraction pattern of both hybrid nanomaterials paves the new way to study the symmetry of *Begomovirus* capsid protein. However, upon analyzing the diffraction pattern, it seems that every point of symmetry on virus capsid possibly embedded by metal nanoparticles principally gave the diffraction orientation pattern where exactly mimics the icosahedral symmetry of *Begomovirus* (Fig. 4E). By indexing the SAED crystal diffraction pattern, it is elegant to predict the number of nucleation sites rendered by SLCCNV capsid (Figs. 3 and 4E). But it requires some comprehensive physical data analysis.

The *in-vitro* cytotoxicity assay (MTT) supports our fabricated nanomaterials that are robust to use for biomedical applications near future. Gold hybrid nanomaterials treated A549 lung cancer cells shown better viability and biocompatible features than silver hybrid nanomaterials treated at the same concentration (Fig. 7). We also identified statistically significant differences between virus protein and its fabricated nanomaterials. However, the purified virus protein shows no significant cytotoxicity level at higher concentrations when compared to both virus fabricated nanomaterials. We, therefore, believe that a combination of bio and inorganic and the relatively large surface area of hybrid nanomaterials were slightly elevated the toxicity level compared to virus particles. These results are consistent with Blandino et al. (2015), who demonstrated no toxicity by plant viruses to human cells. In contrast, both virus fabricated nanomaterials had shown better biocompatibility in low concentrations ranging from 10 to 90 μl (Fig. 7). The 24 h incubation period for virus fabricated nanomaterials is considered as a stringent time duration to study the viability of cells, whereas it would increase if the incubation period reduced from 24 h (Nagvi et al., 2010).

A functional LED light device was fabricated by embedding the SLCCNV-noble metal hybrids and SLCCNV protein in a glass substrate which was connected between two copper electrodes along with the battery (Fig. S1). The embedded materials including, virus protein exhibited electrical conductance switching behaviour were easily detectable by LED light. Tremendously, SLCCNV protein ignites the LED due to its proven electrical conductive capacity. We had never envisaged this result from pure SLCCNV particles that have electrical

conductivity properties. However, it is possible because of the architecture of the virus capsid made of multiple protein monomers which resembles a crystalline arrangement of molecules. There are few similar reports found on peptides that can act as biological conductors (Hauser and Zhang, 2010; Flynn et al., 2003). At the same time, conductivity measurement also provides detailed confirmation about the electrical conductivity properties of SLCCNV templated nanomaterials (Fig. 8A), which make them appear under the semi-conductive band gap since it contains both resistance and conductivity properties (Gagan et al., 2015). A semiconductor is a material which has electrical conductivity to a degree between a conductor and an insulator. E.g., Silicon, Germanium, carbon, etc. (Sze, 2002). Thus, virus templates can be used to produce non-toxic, high semi-conductive organic based nanomaterials. These results suggest that nanoscale virus metallic hybrid material thought to be an indispensable component in future electronics. The nanoscale integrated circuit also produces other fringe benefits. The nanoscale circuits consume less power than conventional circuits, and they cost less to operate. They generate less heat and, therefore, generally do not require elaborate cooling or ventilation systems. The nanoscale circuits are also capable of operating at higher speeds because it takes nanoseconds for signals to travel through them. Their virus hybrid nanomaterials semi-conductivity properties may be altered in useful ways by the controlled deposition of metal ion precursors.

5. Conclusion

It is likely that most virus capsids are more dynamic in structure, rather than static cages, whose transitions are only now being revealed (Whaley et al., 2000). The viral capsid interacts with its environment primarily at the external surface. Modification of the external surfaces with small molecules can direct the cage toward specific interactions with both biological and non-biological surfaces. The repetitive structure of the capsid exterior surface serves as a platform for multivalent presentation, providing a significant advantage over traditional materials processing (Sarikaya et al., 2003; Lewis et al., 2006; Sun et al., 1993). Few viruses displaying nucleation properties have been used as templates for material synthesis. Also, the nucleation peptides identified by phage display can be engineered into another virus and virus-like protein cage architectures for direct nucleation and spatial control over mineral particle growth (Flynn et al., 2003; Porta et al., 2003; Chatterji et al., 2002).

In this research study, we have achieved to fabricate the noble metal nanomaterials using destructive plant pathogenic virus of *Squash leaf curl China virus* as a biotemplate. Both fabricated virus-metallic-hybrid nanomaterials are of great importance while it has synthesised at a high degree of control. All the characteristic features analyzed by instrumental methods provide sufficient information about the virus-hybrid-metallic nanomaterials and have revealed few unique properties. Using SLCCNV biotemplates as a “nanofactory” can produce customized size variant metal nanoparticles depending on the amount of precursor and virus template. Though it can be easily separated from the template, it might be implemented in numerous applications like gene delivery, drug delivery and highly sensitive diagnostic assays where the size

of the particles is crucial. The durability of hybrid nanomaterials towards higher temperature shows as a sensitive part of semi-conductor material which directly impact the conduction band (Varshni, 1967). Intriguingly, the biocompatibility study along with wild SLCCNV and its fabricated hybrid nanomaterial shows good biocompatible features for the first time ever in the history of viral nanotechnology (Steinmetz and Manchester, 2011). In the consequences of the result, we ultimately reached our objective of this research work, that is a virus hybrid nanomaterials have shown good electrical conductivity which was validated by the simple handmade device along with pico-ammeter. Hence, using SLCCNV biotemplate, it is possible to generate a conductive matrix within a few minutes at any place under the direct sunlight which is an important criterion to enable access to advances in semi-conductive material systems. Since naturally occurring viral particles rarely feature the functional groups, SLCCNV can mediate the surface mineralization with its available amino acid residues (Klem et al., 2003; Andrew et al., 2015; Blum et al., 2005; Kramer et al., 2004; Lee et al., 2002).

Therefore, from a materials science point of view, there are many interesting possibilities to be explored using this *Squash leaf curl China virus* combined with inorganic materials to develop new applications which is cost effective, simple and rapid. Remarkably, we discovered some novel characters in many instances on our SLCCNV fabricated hybrid metallic nanomaterials, which may contribute to the advances of virus nanotechnology without any doubt.

Acknowledgments

The authors acknowledge National Centre for Nanoscience and Nanotechnology, University of Madras, Chennai, India, for Nanomaterials characterization. We thank Dr. Ashok Kumar, Department of Nuclear physics, University of Madras, for helping to achieve electrical conductivity testing for our nanomaterials. We immensely thank Dr. G. Dharanivasan, Indian Institute of Technology for helpful discussion and thank Dr. Bupesh Munisamy for help in manuscript improvement.

References

- Ahmad, A., Senapati, S., Khan, M.I., Kumar, R., Ramani, R., Srinivas, V., Sastry, M., 2003. Intracellular synthesis of gold nanoparticles by a novel alkalotolerant actinomycete, *Rhodococcus* species. *Nanotechnology* 14, 824–828.
- Ahmad, A., Senapati, S., Khan, M.I., Kumar, R., Sastry, M., 2005. Extra/intra-cellular, biosynthesis of gold nanoparticles by an alkalotolerant fungus, *Trichothecium* sp. *J. Biomed. Nanotechnol.* 1, 47–53.
- Ai, J., Biazar, E., Jafarpour, M., Montazeri, M., Majdi, A., Aminifard, S., Zafari, M., Akbari, H.R., Rad, H.G., 2011. Nanotoxicology and nanoparticle safety in biomedical designs. *Int. J. Nanomed.* 6, 1117–1127.
- Akhtar, M.S., Panwar, J., Yun, Y.S., 2013. Biogenic synthesis of metallic nanoparticles by plant extracts. *ACS Sustain. Chem. Eng.* 1 (6), 591–602.
- Alexandridis, P., 2011. Gold nanoparticle synthesis, morphology control, and stabilization by functional polymers. *Chem. Eng. Technol.* 14, 15–38.
- Alvin, W.O., Mary, M.M., Andrew, R.B., 2015. Synthesis and Characterization of silver nanoparticles for an undergraduate laboratory. *J. Chem. Edu.* 92 (2), 339–344.

- Andrew, J.L., Valentine, V.M., Olga, V., Jane, S., Igor, V.Y., Natalia, O.K., Michael, E.T., 2015. A genetically modified Tobacco Mosaic Virus that can produce gold nanoparticles from a metal salt precursor. *Front Plant Sci.* 6, 984. <https://doi.org/10.3389/fpls.2015.00984>.
- Balci, S., Bittner, A., Hahn, k., Scheu, C., Knez, A., Wege, C., Jeske, H., Kern, K., 2006. Copper nanowires within the central channel of tobacco mosaic virus particles. *Electrochem. Acta* 51, 6251–6257.
- Bancroft, J.B., Wagner, G.W., Bracker, C.E., 1968. The self-assembly of a nucleic-acid free pseudo top component for a small spherical virus. *Virology* 36 (1), 146–149.
- Blandino, A., Lico, C., Baschieri, S., Barberini, L., Cirotto, C., Blasi, P., Santi, L., 2015. In vitro and in vivo toxicity evaluation of plant virus nanocarriers. *Colloids Surf. B Biointerf.* 6, 129–130.
- Blum, A.S., Soto, C.M., Wilson, C.D., Cole, J.D., Kim, M., 2004. Cowpea mosaic virus as a scaffold for 3-D patterning of gold nanoparticles. *Nano Lett.* 4 (5), 867–870.
- Blum, A.S., Soto, C.M., Wilson, C.D., Brower, T.L., Pollack, S.K., 2005. An engineered virus as a scaffold for three-dimensional self-assembly on the nanoscale. *Small* 1 (7), 702–706.
- Bothner, B., Dong, X.F., Bibbs, L., Johnson, J.E., Siuzdak, G., 1998. Evidence of viral capsid dynamics using limited proteolysis and mass spectrometry. *J. Biol. Chem.* 273 (2), 673–676.
- Briddon, R., Bebford, I., Tsai, J.H., Markham, P., 1996. Analysis of the nucleotide sequence of the treeshopper-transmitted Geminivirus, Tomato pseudo-curly top virus, suggests a recombinant origin. *Virology* 219, 387–394.
- Bromley, K.M., Patil, A.J., Perriman, A.W., Stubbs, G., Mann, S., 2008. Preparation of high quality nanowires by tobacco mosaic virus templating of gold nanoparticles. *J. Mater. Chem.* 18, 4796–4801.
- Cao, B., Xu, H., Mao, C., 2011. Transmission electron microscopy as a tool to image bioinorganic nanohybrids: the case of phage-gold nanocomposites. *Microsc. Res. Technol.* 74, 627–635.
- Chandran, S.P., Chaudhary, M., Pasricha, R., Ahmed, A., Sastry, M., 2006. Synthesis of gold nanotriangles and silver nanoparticles using Aloe vera plant extract. *Biotechnol. Prog.* 22, 577–583.
- Chatterji, A., Burns, L.L., Taylor, S.S., Lomonosoff, G.P., Johnson, J.E., 2002. Cowpea mosaicvirus: from the presentation of antigenic peptides to the display of active biomaterials. *Intervirology* 45, 362–370.
- Clark, M.F., Adams, A.N., 1977. Characteristics of the micro-plate method of enzyme-linked immunosorbent assay for the detection of plant viruses. *J. Gen. Virol.* 34, 475–483.
- Courchesne, N.M.D., Klug, M., Chen, P.Y., Kooi, S.E., Yun, D.S., Hong, N., Fang, N.X., Belcher, A.M., 2014. Assembly of a bacteriophage-based template for the organization of materials into nanoporous networks. *Adv. Mater.* 26, 3398–3404.
- Dameron, C.T., Reeser, R.N., Mehra, R.K., Kortan, A.R., Carroll, P. J., Steigerwald, M.L., Brus, L.E., Winge, D.R., 1989. Biosynthesis of cadmium sulphide quantum semiconductor crystallites. *Nature* 338, 596–597.
- Douglas, T., Young, M., 1998. Host guest encapsulation of materials by assembled virus protein cages. *Nature* 393, 152–155.
- Dujardin, E., Peet, C., Stubbs, G., Culvar, J.N., Mann, S., 2003. Organization of metallic nanoparticles using Tobacco mosaic virus. *Nano Lett.* 3, 413–417.
- Eustis, S., Hsu, H.Y., El-Sayed, M.A., 2005. Gold nanoparticle formation from photochemical reduction of Au³⁺ by continuous excitation in colloidal solutions: a proposed molecular mechanism. *J. Phys. Chem. B* 109, 4811–4815.
- Fischlechner, M., Donath, E., 2007. Viruses as building blocks for materials and devices. *Angew. Chem.* 46 (18), 3184–3193.
- Flenniken, M.L., Uchida, M., Lipold, L., Kang, S., Young, M.J., Douglas, T., 2009. A library of protein cage architectures as nanomaterials. *Curr. Top. Microbiol. Immunol.* 327, 71–73.
- Flynn, C.E., Mao, C.B., Hayhurst, A., Williams, J.L., Georgiou, G., 2003. Synthesis and organization of nanoscale II–VI semiconductor materials using evolved peptide specificity and viral capsid assembly. *J. Mater. Chem.* 13, 2414–2421.
- Gagan, K., Raju, A., Peter, C., Mark, B., Pathiraja, G., 2015. Electrically conductive polymers and composites for biomedical applications. *RSC Adv.* 5 (37553), 37567.
- Gholami-Shabani, M., Shams-Ghahfarokhi, M., Gholami-Shabani, Z., Akbarzadeh, A., Riazi, G., Ajdari, S., Amani, A., 2015. Enzymatic synthesis of gold nanoparticles using sulfite reductase purified from *Escherichia coli*: a green eco-friendly approach. *Process Biochem.* 50 (7), 1076–1085.
- Han, X.X., Zhao, B., Ozaki, Y., 2009. Surface-Enhanced Raman spectroscopy. *Anal. Bioanal. Chem.* 394 (7), 1719–1727.
- Hauser, Charlotte A.E., Zhang, Shuguang, 2010. Nanotechnology: Peptides as biological semi-conductors. *Nature* 468, 516–517.
- Husseiny, M.I., El-Aziz, M.A., Badr, Y., Mahmoud, M.A., 2007. Biosynthesis of gold nanoparticles using *Pseudomonas aeruginosa*. *Spectrochim. Acta A* 67, 1003–1006.
- Jain, N., Bhargava, A., Majumdar, S., Panwar, J., 2011. Extracellular biosynthesis and characterization of silver nanoparticles using *Aspergillus flavus* NJP08: a mechanism prospective. *Nanoscale* 3 (2), 635–641.
- Joerger, T.K., Joerger, R., Olsson, E., Granqvist, C.G., 2001. Bacteria as workers in the living factor: Metal accumulating bacteria and their potential for materials science. *Trends Biotechnol.* 19 (1), 15–20.
- Kale, A., Bao, Y., Zhou, Z., Prevelige, P.E., Gupta, A., 2013. Directed self-assembly of CdS quantum dots on bacteriophage P22 coat protein templates. *Nanotechnology* 24 (4), 045603.
- Kaumeel, C., Imran, P., Tonmoy, G., Chetan, P., Rahulkumar, M., Anup, C., Sandhya, M., 2016. Green synthesis, characterization and antioxidant potential of silver nanoparticles biosynthesized from de-oiled biomass of thermotolerant oleaginous microalgae, *Acutodesmus dimorphus*. *RSC Adv.* 6, 72269–72274.
- Kevin, G.S., Juan, C., 2011. Optimal size of silver nanoparticles for surface-enhanced raman spectroscopy. *J. Phys. Chem. C* 115, 1403–1409.
- Khan, A.A., Fox, E.K., Gorzny, M.L., Nikulina, E., Brougham, D.F., Wege, C., Bittner, A.M., 2013. pH control of the electrostatic binding of gold and iron oxide nanoparticles to Tobacco mosaic virus. *Langmuir* 29 (7), 2094–2098.
- Klem, M.T., Willits, D., Young, M., Douglas, T., 2003. 2-D array formation of genetically engineered viral cages on Au surfaces and imaging by atomic force microscopy. *J. Am. Chem. Soc.* 125, 10806–10807.
- Klem, M.T., Willits, D., Solis, D.J., Belcher, A.M., Young, M., Douglas, T., 2005. Bio-inspired synthesis of protein-encapsulated CoPt nanoparticles. *Adv. Funct. Mater.* 15, 1489–1494.
- Knez, M.T., Bittner, A.M., Wege, C., Jeske, h., Martin, T.P., Kern, 2004. Spatially selective nucleation of metal clusters on the tobacco mosaic virus. *Adv. Funct. Mater.* 14 (2), 116–124.
- Kowshik, M., Arhtaputre, S., Kharrazi, S., Vogel, W., Urban, J., Kulkarni, S.K., Paknikar, K.M., 2003. Extracellular synthesis of silver nanoparticles by a silver-tolerant yeast strain MKY3. *Nanotechnology* 14, 95–100.
- Kramer, R.M., Li, C., Carter, D.C., Stone, M.O., Naik, R.R., 2004. Engineered protein cages for nanomaterial synthesis. *J. Am. Chem. Soc.* 126, 13282–13286.
- Kuber, C.B.D., Souza, S.F., 2006. Extracellular biosynthesis of silver nanoparticles using the fungus *Aspergillus fumigatus*. *Colloids Surf. B* 47, 160–164.
- Kulkarni, N., Muddapur, U., 2014. Biosynthesis of metal nanoparticles: a review. *J. Nanotechnol.* <https://doi.org/10.1155/2014/510246>.
- Kumar, P., Singh, P., Kumari, K., Mozumdar, S., Chandra, R., 2011. A green approach for the synthesis of gold nanotriangles using aqueous leaf extract of *Callistemon viminalis*. *Mater. Lett.* 65, 595–597.
- Laemml, U.K., 1970. Cleavage of structural protein during the assembly of the head of bacteriophage T4. *Nature* 227 (5259), 680–685.

- Lazarowitz, S.G., 1987. The molecular characterization of geminiviruses. *Plant Mol. Biol. Rep.* 4, 177–192.
- Lee, S.W., Mao, C., Flynn, C.E., 2002. Belcher A.M. Ordering of quantum dots using genetically engineered viruses. *Science* 296, 892–895.
- Lee, Y.J., Yi, H., Kim, W.J., Kang, K., Yun, D.S., Strano, M.S., Ceder, G., Belcher, A.M., 2009. Fabricating genetically engineered high-power lithium-ion batteries using multiple virus gene. *Science* 324 (5930), 1051–1055.
- Lewis, J.D., Destito, G., Zijlstra, A., Gonzalez, M.J., Quigley, J.P., 2006. Viral nanoparticles as tools for intravital vascular imaging. *Nat. Med.* 12, 354–360.
- Luisoni, E., Milne, R.G., Vecchiati, M., 1995. Purification of tomato yellow leaf curl geminivirus. *New Microbiol.* 18, 253–260.
- Mao, C., Solis, D.J., Reiss, B.D., Kottmann, S.T., Sweeney, R.Y., 2004. Virus-based toolkit for the directed synthesis of magnetic and semiconducting nanowires. *Science* 303, 213–217.
- Merzlyak, A., Lee, S.W., 2006. Phage as template for hybrid materials and mediators for nanomaterials synthesis. *Curr. Opin. Chem. Biol.* 10, 246–252.
- Mohanpuria, P., Rana, N.K., Yadav, S.K., 2008. Biosynthesis of nanoparticles: technological concepts and future applications. *J. Nanopart. Res.* 10, 507–517.
- Monaliben, S., Derek, F., Shashi, S., Suraj, K., Tripathy, Gerrard, E.J. P., 2015. Green synthesis of metallic nanoparticles via biological entities. *Materials* 8, 7278–7308.
- Mosman, T., 1983. Rapid Colorimetric Assay for cellular growth and survival: application to proliferation and cytotoxicity assays. *J. Immunol. Methods* 65, 55–63.
- Mukherjee, P., Ahmad, A., Mandal, D.S., Senapati, S., Sainkar, R., Khan, M.I., Parishcha, R., Aiayumar, P.V., Alam, M., Kumar, R., 2001. Fungus-mediated synthesis of silver nanoparticles and their immobilization in the mycelia matrix: a novel biological approach to nanoparticles synthesis. *Nano Lett.* 1, 515–519.
- Nagvi, S., Samim, M., Abidin, M., Ahmed, F.J., Maitra, A., Prashant, C., Dinda, A.K., 2010. Concentration-dependent toxicity of iron oxide nanoparticles mediated by increased oxidative stress. *Int. J. Nanomed.* 5, 983–989.
- Nair, B., Pradeep, T., 2002. Coalescence of nanoclusters and formation of submicron crystallites assisted by *Lactobacillus* strains. *Cryst. Growth Des.* 2 (4), 293–298.
- Nam, K.T., Kim, D.W., Yoo, P.J., Chiang, C.Y., Meethong, N., Hammond, P.T., Chiang, Y.M., Belcher, A.M., 2006. Virus-enabled synthesis and assembly of nanowires for lithium ion battery electrodes. *Science* 312 (5775), 885–888.
- Namba, K., Stubbs, G., 1986. Structure of tobacco mosaic virus at 3.6Å resolution: implication for assembly. *Science* 231 (4744), 1401–1406.
- Nguyen, T.K.T., Maclean, N., Mahiddine, S., 2014. Mechanisms of Nucleation and growth of nanoparticles in solution. *Chem. Rev.* 114, 7610–7630.
- Njagi, E.C., Huang, H., Stafford, L., Genuino, H., Galindo, H.M., Collins, J.B., Hoag, G.E., Suib, S.L., 2011. Biosynthesis of iron and silver nanoparticles at room temperature using aqueous sorghum bran extracts. *Langmuir* 27 (1), 264–271.
- Pedro, H.C. Camargo, Thenner, S. Rodrigues, Anderson, G.M., da Silva, Jiale, W., 2015. Controlled synthesis: nucleation and growth in solution. *Metall. Nanostruct.* 47–49. <https://doi.org/10.007/978-3-319-11304-3>.
- Philip, D., 2010. Green synthesis of gold and silver nanoparticles using *Hibiscus rosa sinensis*. *Physica E* 42, 1417–1424.
- Porta, C., Spall, V.E., Findlay, K.C., Gergerich, R.C., Farrance, C.E., Lomonosoff, G.P., 2003. Cowpea mosaic virus based chimaeras effects of inserted peptides on the phenotype, host range, and transmissibility of the modified viruses. *Virology* 310 (1), 50–63.
- Pratibha, R., 2009. Protein-mediated synthesis of gold nanoparticles. *Mater. Sci. Eng.: B* 163 (2), 93–98.
- Raja Muthuramlingam, T., Chandrasekar, S., Dharanivasan, G., Nallusamy, D., Rajendran, N., Kathiravan, K., 2015. Bioactive bile salt capped silver nanoparticles activity against destructive plant pathogenic fungi through *invitro* system. *RSC Adv.* 5, 71174.
- Raja Muthuramlingam, T., Dharanivasan, G., Michael, I.J., Deepan, S., Mohammed Riyaz, S.U., Kathiravan, K., 2016. Nanobiotechnological approach using plant rooting hormones synthesized silver nanoparticle as a “nanobullets” for the dynamic applications in horticulture – an in vitro and ex vitro study. *Arab. J. Chem.* 11 (1), 48–61.
- Riyaz, M.S.U., Deepan, S., Dharanivasan, G., Jesse, M.I., Raja Muthuramalingam, T., Kathiravan, K., 2013. First report on a varetiant of Squash leaf curl China virus (SLCCNV) infecting *Benincasa hispida* in India. *New Dis. Rep.* 28, 20.
- Ruoslahti, E., 2000. Targeting tumor vasculature with homing peptides from phage display. *Semin. Cancer Biol.* 10 (6), 435–442.
- Sanctis, S., Hoffmann, R.C., Eiben, S., Schneider, J.J., 2015. Microwave assisted synthesis and characterization of a Zinc oxide/tobacco virus hybrid material. An active hybrid semiconductor in a field-effect transistor device. *Beilstein J. Nanotechnol.* 6, 785–791.
- Sarikaya, M., Tamerler, C., Jen, A.Y., Schulten, K., Baneyx, F., 2003. Molecular biomimetics: nanotechnology through biology. *Nat. Mater.* 2, 577–585.
- Sastry, M., Ahmad, A., Khan, M.I., Kumar, R., 2003. Biosynthesis of metal nanoparticles using fungi and actinomycete. *Curr. Sci.* 85 (2), 162–170.
- Satish, K., Nune, Nripen C.R., Kavita, S., Rajesh, K., Kulkarni Subramanian, T., 2009. Green nanotechnology from tea: phytochemicals in tea as building blocks for production of biocompatible gold nanoparticles. *J. Mater. Chem.* 19, 2912–2920.
- Schneider, C.A., Rasband, W.S., Eliceiri, K.W., 2012. NIH Image to ImageJ: 25 years of image analysis. *Nat. Methods* 9 (7), 671–675.
- Scholthof, K.B., Adkins, S., Czosnek, H., Palukaitis, P., Jacquot, E., Hohn, T., Hohn, B., Saunders, K., Candresse, T., Ahlquist, P., Hemenway, C., Foster, G.D., 2011. Top 10 plant viruses in molecular plant pathology. *Mol. Plant Pathol.* 12 (9), 938–954.
- Segtnan, V.H., Hildrum, K.I., Wold, J.P., 2009. New methods for analysis of factors affecting meat eating quality. In: Woodhead Publishing Series in Food Science, Technology and Nutrition, Improving the Sensory and Nutritional Quality of Fresh Meat. Woodhead Publishing, pp. 519–538. <https://doi.org/10.1533/9781845695439.4.519> (ISBN 9781845693435).
- Seongmin, H., Xiao, L., 2013. Optimal size of gold nanoparticles for surface enhanced raman spectroscopy under different conditions. *J. Nanomater.* <https://doi.org/10.1155/2013/790323>.
- Singh, R., Raj, S.K., Prasad, V., 2008. Molecular Characterization of a Strain of Squash leaf curl China Virus from North India. *J. Phytopathol.* 156 (4), 222–228.
- Sirotkin, S., Mermet, A., Bergoin, M., Ward, V., Van Etten, J.L., 2014. Viruses as nanoparticles: structure versus collective dynamics. *Phys. Rev. E* 90, 022718.
- Steinmetz, N.F., Manchester, M., 2011. Viral Nanoparticles: Tools for Materials Science and Biomedicine. Pan Stanford Publishing Pte. Ltd..
- Sun, Y., Hegamyer, G., Colburn, N.H., 1993. PCR-direct sequencing of a GC-rich region by inclusion of 10% DMSO: application to mouse c-jun. *Biotechniques* 15 (3), 372–374.
- Susmit, P., Meghna, N., 2015. New era of electronic components: concept of bio-semiconductors. *IJEEE* 7, 01.
- Sze, S.M., 2002. Semiconductor Devices. John Wiley and Sons, pp. 29–31.
- Tan, Y.N., Lee, J.Y., Wang, D.I.C., 2010. Uncovering the design rules for peptide synthesis of metal nanoparticles. *J. Am. Chem. Soc.* 132, 5677–5686.
- Tanford, C., 1961. The interpretation of hydrogen ion titration curves of proteins. *Adv. Protein. Chem.* 17, 69–195.

- Varma, A., Malathi, V.G., 2003. Emerging geminivirus problems: a serious threat to crop production. *Ann. Appl. Biol.* 142 (2), 145–164.
- Varshni, Y.P., 1967. Temperature dependence of the energy gap in semiconductors. *Physica* 34 (1), 149–154.
- Wang, Q., Lin, T.W., Tang, L., Johnson, J.E., Finn, M.G., 2002. Icosahedral virus particles as addressable nanoscale building blocks. *Angew. Chem. Int. Ed.* 41 (3), 459–462.
- Watanabe, H., Hayazawa, N., Inouye, Y., Kawata, S., 2005. DFT vibrational calculations of Rhodamine 6G adsorbed on silver: analysis of tip-enhanced spectroscopy. *J. Phys. Chem. B* 109 (11), 5012–5020.
- Whaley, S.R., English, D.S., Hu, E., Barbara, P.F., Belcher, A.M., 2000. Selection of peptides with semiconductor binding specificity for directed nanocrystal assembly. *Nature* 405 (6787), 665–668.
- Wilson, A.P., 2000. *Cytotoxicity and Viability Assays in Animal Cell Culture: A Practical Approach*. Oxford University Press, Oxford.
- Wolfgang, H., Nguyen, T.K.T., Jenny, A., David, G.F., 2007. Determination of size and concentration of gold nanoparticles from UV-Vis spectra. *Anal. Chem.* 79 (11), 4215–4225.
- Xiao, Z., Fan, Ekaterina, P., Markus, G., Adam, B., Konstantinos, G., Matthew, M., James, C., Reza, G., 2013. Tobacco mosaic virus: A biological building block for micro/nano/bio systems. *J. Vacuum Sci. Technol. A: Vacuum, Surf. Films* 31, 050815. <https://doi.org/10.1116/1.4816584>.
- Xu, L.J., Zong, C., Zheng, X.S., Hu, P., Feng, J.M., Ren, B., 2014. Label-free detection of native protein by surface enhanced Raman spectroscopy using iodide-modified nanoparticles. *Anal. Chem.* 86, 2238–2245.
- Young, M., Willits, D., Uchida, M., Douglas, T., 2008. Plant viruses as biotemplates for materials and their use in nanotechnology. *Annu. Rev. Phytopathol.* 46, 361–384.